IV. Calculation of toroidal rotation profiles in DIII-D using neoclassical viscosity (DoE Grant ER54538)

W. M. Stacey, R. W. Johnson and J. Mandrekas

(to be published in Physics of Plasmas, 2006)

Abstract

Momentum and particle balance and neoclassical viscosity were applied to calculate the radial profile of toroidal rotation in several DIII-D [J. Luxon, Nucl. Fusion, 42, 614 (2002)] discharges in a variety of energy confinement regimes (Low-mode, Low-mode with Internal Transport Barrier, High-mode, and High-mode with Quiescent Double Barrier). Calculated toroidal rotation velocities were found to over-predict measured values most in the center—by factors of 1.5 to 3--with the over-prediction generally decreasing with increasing radius, for the L, H and ITB mode shots, but the single impurity species approximation could not properly model the multiple Ni and Cu charge states in the QDB shots.

I. Introduction

There have been longstanding experimental[1-10] and theoretical[11-27] efforts to characterize and understand toroidal rotation and the related radial transport of angular momentum in neutral beam driven tokamaks. Since the theoretical expression for the toroidal rotation velocity follows directly from toroidal momentum balance once the viscous stress is specified, understanding toroidal rotation is primarily a matter of understanding toroidal viscosity.

It was early noted that the familiar "perpendicular" viscosity of classical theory was much too small to account for observed momentum damping[1,13-15], even when extended to take neoclassical effects into account[13-15,18,19], giving rise to the now widespread belief that momentum transport in tokamaks was "anomalous". The observation in several recent experimental investigations[4,5,7,8,10,28] that the ratio of the inferred momentum diffusivity and ion thermal diffusivity (χ_ϕ / χ_i), or the ratio of parameters that are determined by these diffusivities, was relatively uniform over the radial dimension of the plasma was interpreted as further evidence that the momentum transport was anomalous, since the ion thermal transport was believed to be anomalous in these discharges.

It was also early pointed out[11,12] (but little noted) that there was a second, gyroviscous contribution to the radial transport of angular momentum in classical theory with a gyroviscosity coefficient that was several orders of magnitude larger than the perpendicular viscosity coefficient. The relative obscurity of the gyroviscous contribution in momentum transport analyses (it has long been included in extended MHD codes such as NIMROD and M3D) is perhaps due in part to the fact that it vanishes in cylindrical geometry (hence would not have survived in much of the early theoretical work) and in part by its puzzling failure to survive in some contemporary developments of neoclassical viscosity based on a formal gyroradius ordering of the flow fields[18,19,26], which essentially recovered the much smaller classical perpendicular viscosity with small corrections. In any case, there would now appear to be a firm theoretical basis for gyroviscosity[11,12,16,17,20-25,27]. It is our purpose in this paper to test neoclassical viscosity by using neoclassical gyroviscosity to calculate the radial profile of toroidal rotation velocity and neoclassical parallel viscosity to poloidal density and velocity asymmetries that are needed to evaluate the gyroviscous torque for comparison with measured values in a set of DIII-D discharges.

We would anticipate that there are other, non-classical momentum transport mechanisms present in DIII-D (and other) discharges (e.g. Ref. 29). However, since the particle motions and forces that give rise to classical and neoclassical transport are always present (trapped particle effects only in the appropriate collisionality regimes), it is important to make a comparison of the predictions of neoclassical momentum transport theory with rotation measurements in order to establish the magnitude of the additional transport that must be accounted for by these other transport mechanisms.

For this purpose, we make use of the practical computation formalism that has been developed by extending the Braginskii gyroviscosity formalism to tokamak toroidal flux surface geometry[17] (i.e. the "Pfirsch-Schluter" extension of classical gyroviscosity) and by developing a methodology for evaluating the poloidal asymmetry factors needed to determine the rate of radial transport of toroidal angular momentum[20]. A number of previous, less extensive, comparisons of this formalism with experimental data[30-32] have established that gyroviscosity predicts the magnitude of the global momentum loss rate (the

momentum confinement time) in many neutral beam driven tokamaks and under a variety of operating conditions. The intent of this paper is to extend these investigations to test the ability of this gyroviscosity formalism to predict the radial profile, as well as the overall magnitude, of the radial transport rate of toroidal angular momentum for neutral beam driven DIII-D plasmas in a variety of energy confinement regimes.

Radial momentum transport in tokamak plasmas is of intrinsic interest, of course, for what it reveals about basic transport processes. Moreover, toroidal rotation has also been shown to affect neoclassical particle transport[33,34], to suppress MHD resistive wall mode instabilities[35-37], and to alter MHD equilibria[38], and is postulated to be involved in the shear suppression of transport enhancing microinstabilities[39].

II. Neoclassical Radial Transport of Toroidal Angular Momentum

A. Viscous torques

Following the previous generalization[17] of the Braginskii[12] derivation to toroidal flux-surface geometry, the toroidal component of the viscous torque can be written

$$R^2\nabla\phi\cdot\nabla\cdot\Pi = \frac{1}{Rh_p}\frac{\partial}{\partial l_\psi}(R^2 h_p \Pi_{\psi\phi}) + B_p\frac{\partial}{\partial l_p}\left(\frac{R\Pi_{p\phi}}{B_p}\right) \tag{1}$$

where the Π_{pq} are the stress tensor elements that result from the Braginskii decomposition of the rate-of-strain tensor extended to a right-hand 'radial', 'poloidal', toroidal (ψ, p, ϕ) flux-surface coordinate system with length elements $(dl_\psi = h_\psi d\psi, dl_p = h_p dp, dl_\phi = h_\phi d\phi)$. The viscous stress tensors have 'perpendicular' components

$$\Pi^{\perp}_{\psi\phi} = -\eta_2 R\frac{\partial}{\partial l_\psi}\left(V_\phi/R\right), \Pi^{\perp}_{p\phi} = -\eta_2 R\frac{\partial}{\partial l_p}\left(V_\phi/R\right) \tag{2}$$

gyroviscous components

$$\Pi^{gv}_{\psi\phi} = -\eta_4 R\frac{\partial}{\partial l_p}\left(V_\phi/R\right), \Pi^{gv}_{p\phi} = -\eta_4 R\frac{\partial}{\partial l_\psi}\left(V_\phi/R\right) \tag{3}$$

and 'parallel' viscous components

$$\Pi^{\parallel}_{\psi\phi} = 0, \Pi^{\parallel}_{p\phi} = -\frac{3}{2}\eta_0 f_p A_0 \tag{4}$$

where

$$A_0 = 2\left\{-\frac{1}{3}\left(\frac{\partial V_p}{\partial l_p}\right) + \left[\left(\frac{1}{R}\right)\frac{\partial R}{\partial l_p} + \frac{1}{3}\left(\frac{1}{B_p}\right)\frac{\partial B_p}{\partial l_p}\right]V_p + f_p R\frac{\partial\left(V_\phi/R\right)}{\partial l_p}\right\} \tag{5}$$

and $f_p = B_p/B_\phi$.

The Braginskii values of the viscosity coefficients in a collisional plasma are

$$\eta_0 = nT\tau, \eta_4 = nTm/ZeB = \eta_0/\Omega\tau, \eta_2 = \eta_4/\Omega\tau = \eta_0/(\Omega\tau)^2 \tag{6}$$

where τ is the self-collision time and $\Omega=m/ZeB$ is the gyrofrequency. Since typically $\Omega\tau \approx 10^3 - 10^4$, $\eta_0 >> \eta_4 >> \eta_2$. Taking into account trapped particle effects that would occur at lower collisionality should not directly effect η_4, which has no τ-dependence, and has been shown[18,19] to have very little effect on η_2. However, trapped particle effects at lower collisionality have a major effect on η_0, which we represent as[31]

$$\eta_{0j} = \frac{n_j m_j \upsilon_{thj} qR\varepsilon^{-3/2}\nu_{jj}^*}{\left(1+\varepsilon^{-3/2}\nu_{jj}^*\right)\left(1+\nu_{jj}^*\right)} \equiv n_j m_j \upsilon_{thj} qR f_j\left(\nu_{jj}^*\right) \tag{7}$$

where $\nu_{jj}^* = \nu_{jj} qR/\upsilon_{thj}$, υ_{thj} is the thermal speed, q is the safety factor, and $\varepsilon=r/R$.

Since the flux surface average of the second term in Eq.(1) vanishes identically, and the 'parallel' component of the first term in Eq. (1) vanishes identically, the flux surface averaged toroidal viscous torque may be written as the sum of the gyroviscous and perpendicular viscous components

$$\left\langle R^2\nabla\phi\cdot\nabla\cdot\Pi\right\rangle = \left\langle R^2\nabla\phi\cdot\nabla\cdot\Pi\right\rangle_{gv} + \left\langle R^2\nabla\phi\cdot\nabla\cdot\Pi\right\rangle_{\perp} \tag{8}$$

where

$$\left\langle R^2\nabla\phi\cdot\nabla\cdot\Pi\right\rangle_{gv} = -\left\langle \frac{1}{Rh_p}\frac{\partial}{\partial l_\psi}\left(R^3 h_p \eta_4 \frac{\partial}{\partial l_p}\left(V_\phi/R\right)\right)\right\rangle \tag{9}$$

and

$$\left\langle R^2\nabla\phi\cdot\nabla\cdot\Pi\right\rangle_{\perp} = -\left\langle \frac{1}{Rh_p}\frac{\partial}{\partial l_\psi}\left(R^3 h_p \eta_2 \frac{\partial}{\partial l_\psi}\left(V_\phi/R\right)\right)\right\rangle \tag{10}$$

If the plasma rotated as a rigid body, $\Omega \equiv V_\varphi/R \neq \Omega(\psi,p)$, then both of these components of the viscous torque would vanish identically. It is departure from rigid body rotation in the flux surface, $\Omega = \Omega(p)$, that drives the gyroviscous torque, and departure from rigid body rotation radially, $\Omega = \Omega(\psi)$, that drives the perpendicular viscous torque. Although the radial departure of the toroidal rotation velocity from rigid body rotation is generally larger by an order of magnitude or more than the poloidal departure of the toroidal rotation velocity from rigid body rotation in the flux surface, the gyroviscosity coefficient is larger than the perpendicular viscosity coefficient by 3-4 orders of magnitude, $\eta_4 \approx (\Omega\tau)\eta_2 \approx (10^3\text{-}10^4)\eta_2$, so that the gyroviscous toroidal torque is generally a couple of orders of magnitude larger than the perpendicular toroidal viscous torque. We note again that it is the smaller, perpendicular toroidal viscous torque to which several authors were referring when they stated that the neoclassical viscosity is too small to account for experimentally observed rotation damping.

Finally, we further note that it has been suggested[23] that the above expression for the gyroviscous toroidal torque, which is based on the Braginskii development of the viscous stress tensor, may overestimate the momentum transport rate in regions of steep pressure gradients and low toroidal rotation (e.g. the plasma edge pedestal) because of the $V_\phi \sim \upsilon_{th}$ ordering of the Braginskii derivation[12]. Mikhailovskii and Tsypin[16] were the first, and Catto and Simakov[27] the most recent, to repeat the Braginskii derivation in the $V_\phi << \upsilon_{th}$ ordering. Braginskii's derivation, which is used in this paper, is valid if the fluid velocities in the directions perpendicular and parallel to **B** are larger than the diamagnetic velocity and the diamagnetic velocity multiplied by B_φ/B_p, respectively[25]. If this condition is not satisfied, then a heat flux term may be required also in the parallel, perpendicular and gyroviscous torque expressions[25,27]. This 'large rotation' condition for the validity of the Braginskii ordering appears to be valid over most of the radius for the discharges considered in this paper, as will be discussed later.

B. Toroidal viscous torque approximate representation

In order to obtain an approximate model for numerically evaluating the gyroviscous torque on each flux surface separately, we specialize to toroidal geometry, use the representations $B = B^0/(1+\varepsilon\cos\theta), R = R_0(1+\varepsilon\cos\theta)$, replace the radial gradients in Eq. (9) by radial gradient scale lengths (e.g. $L_n^{-1} = -1/n\,\partial n/\partial r$) which will be evaluated from experiment in this paper, and expand the poloidal dependence of densities and velocities in a low-order Fourier series of the form

$$n_j(r,\theta) = n_j^0\left[1 + n_j^c(r)\cos\theta + n_j^s(r)\sin\theta\right] \tag{11}$$

to obtain a representation of the toroidal viscous torque in terms of an angular momentum transfer, or "drag", frequency, ν_{dj}

$$\left\langle R^2\nabla\phi\cdot\nabla\cdot\boldsymbol{\pi}_j\right\rangle_{gv} \equiv \frac{1}{2}\tilde{\theta}_j G_j \frac{n_j m_j T_j}{e_j B_\phi}\frac{V_{\phi j}^0}{\overline{R}} \equiv R n_j m_j \nu_{dj} V_{\phi j}^0 \tag{12}$$

where

$$\begin{aligned}\tilde{\theta}_j &\equiv \left(4+\tilde{n}_j^c\right)\hat{V}_{\phi j}^s + \tilde{n}_j^s\left(1-\hat{V}_{\phi j}^c\right)\\ &= \left(4+\tilde{n}_j^c\right)\left(-\left(\hat{V}_{\theta j}/\hat{V}_{\phi j}\right)\left(\hat{\Phi}^s + \tilde{n}_j^s\right) + \hat{\Phi}^s\left(1+\left(\hat{P}_j'/\hat{V}_{\phi j}\right)\right)\right) +\\ &\quad \tilde{n}_j^s\left(\left(\hat{V}_{\theta j}/\hat{V}_{\phi j}\right)\left(\hat{\Phi}^c + \tilde{n}_j^c + 2\right) - \hat{\Phi}^c\left(1+\left(\hat{P}_j'/\hat{V}_{\phi j}\right)\right)\right)\end{aligned} \tag{13}$$

represents poloidal asymmetries and

$$G_j \equiv -\frac{r}{\eta_{4j}V_{\phi j}}\frac{\partial\left(\eta_{4j}V_{\phi j}\right)}{\partial r} = r\left(L_n^{-1} + L_T^{-1} + L_{V_\phi}^{-1}\right) \tag{14}$$

represent radial gradients. We have used the gyroviscosity coefficient $\eta_{4j} \approx n_j m_j T_j/e_j B$ and introduced the notation

$$\hat{V}_{\theta j} \equiv \frac{V_{\theta j}^0}{f_p \upsilon_{thj}},\ \hat{V}_{\phi j} \equiv \frac{V_{\phi j}^0}{\upsilon_{thj}},\ \hat{P}_j' \equiv \frac{1}{n_j^0 e_j B_\theta^0 \upsilon_{thj}}\frac{\partial\overline{p_j}}{\partial r},\ f_p \equiv \frac{B_\theta}{B_\phi},\ \tilde{n}_j^{c/s} \equiv \frac{n_j^{c/s}}{\varepsilon},\ \hat{\Phi}^{c/s} \equiv \frac{\Phi^{c/s}}{\varepsilon} = \frac{n_e^{c/s}}{\varepsilon\left(e\Phi/T_e\right)} \tag{15}$$

with the last relation following from electron momentum balance, and neglected radial gradients in the density asymmetry coefficients $n_j^{c,s}$. The radial gradient scale lengths needed to evaluate the G_j from Eq. (14) are taken from experiment in this paper.

C. "Neoclassical" terminology and collisionality dependence

The terminology "neoclassical" is used differently by various authors, and the collisionality dependence of the neoclassical viscosity is subtle, so a brief discussion of both is in order. Transport due to collisions in straight field-line geometry (e.g. cylinders) is referred to as "classical" transport. Kaufman[11] and Braginskii[12] worked out a "classical" theory of viscosity. In the more familiar case of Braginski, the viscosity was derived from kinetic theory under the assumption of large collisionality and large rotation $V_\phi \gg \upsilon_{th}$.

Extension of "classical" Braginskii collisional transport to include the effects of toroidal geometry is referred to in this paper, but not by all authors, as "neoclassical" transport (i.e. Pfirsch-Schluter transport). In general, collisional transport in toroidal geometry includes the "classical" transport plus the new "neoclassical" transport effects due to the toroidal geometry. Since the latter effects are larger, the "classical" transport is usually neglected in toroidal geometry relative to the new Pfirsh-Schluter "neoclassical" transport, but it is still there (i.e. the forces producing it are still operable).

Mikhailovskii and Tyspin[16], Stacey and Sigmar[17] and recently Catto and Simakov[27] extended "classical" viscosity theory to toroidal geometry to obtain what we refer to in this paper as a "neoclassical viscosity" theory that takes into account Pfirsch-Schluter-like toroidal geometry effects.

We note that this "Pfirsch-Schluter gyroviscosity" vanishes to leading order in the absence of an up-down asymmetry in either the density or the toroidal rotation velocity[17], as shown explicitly in Eq. (13), but survives at higher order[27]. This does not mean that gyroviscosity vanishes in a tokamak with an up-down symmetric magnetic field structure, because inertial and other effects can produce up-down density and rotation velocity asymmetries even in tokamaks with an up-down symmetric magnetic field structure[20,30-32]. Catto and Simakov[27] recently concluded purely on theoretical grounds that sufficiently strong up-down asymmetries such as found in diverted plasmas could drive gyroviscous momentum transport rates comparable to those observed experimentally, but did not note that similarly strong up-down asymmetries could be produced by inertial and other effects (see Fig. 3).

At sufficiently small collisionality, trapped particle effects introduce additional transport effects in toroidal geometry that are usually larger than the Pfirsh-Schluter transport effects (at least for the more familiar heat conductivities), although the latter (and also the "classical" transport effects) are still present because most of the particles are untrapped. We refer to the transport associated with these trapped particle effects also as "neoclassical" transport, while noting that some authors refer to it as "banana-plateau" transport, and that yet other authors refer to only these trapped particle transport effects as "neoclassical". Numerous authors have investigated trapped particle effects on the parallel component of the viscosity tensor and found them to cause a significant enhancement of the viscosity coefficient [Eq. (7) is one such example], but of course to exist only when the collisionality was small enough to allow a small number of trapped particles to execute trapped particle orbits. Hinton and Wong[18] (and others) worked out the trapped particle effects on the perpendicular component of the viscosity and found only a small enhancement over the "classical" Braginskii value.

The Pfirsch-Schluter-like "neoclassical gyroviscosity" of this paper does not have any explicit collisionality dependence, and no one has suggested that there is any direct trapped particle effect on gyroviscosity, to our knowledge. This does not mean that the Pfirsch-Schluter-like gyroviscosity does not exist in low collisionality plasmas, only that trapped particle effects do not directly enhance gyroviscosity relative to the "neoclassical Pfirsch-Schluter" values produced by toroidal geometry effects. However, since trapped particle effects enhance the parallel component of viscosity [Eq. (7)] that is used in solving the poloidal momentum moments equations [Eqs. (19)-(22)] for the poloidal velocities and density asymmetries needed to evaluate the gyroviscous torque from Eqs. (12)-(14), there is an indirect trapped particle collisionality dependence of gyroviscosity that is taken into account in the calculation of this paper.

D. Poloidal rotation velocities and density asymmetries

Evaluation of the poloidal asymmetry factors $\widetilde{\theta}_j$ of Eq. (13) requires the solution of the poloidal momentum balance equations for the poloidal rotation velocities and the poloidal density asymmetries.

The poloidal component of the momentum balance equation is

$$n_j m_j \left[\left(\mathbf{V}_j \cdot \nabla \right) \mathbf{V}_j \right]_\theta + \left[\nabla \cdot \Pi_j \right]_\theta + \frac{1}{r} \frac{\partial p_j}{\partial \theta} - M_{\theta j} - F_{\theta j} + n_j e_j \left(V_{rj} B_\phi - E_\theta \right) = 0 \tag{16}$$

where the poloidal components of the inertial and viscous terms are

$$n_j m_j \left[\left(\mathbf{V}_j \cdot \nabla \right) \mathbf{V}_j \right]_\theta = n_j m_j \left[V_{rj} \frac{\partial V_{\theta j}}{\partial r} + \frac{V_{rj} V_\theta}{r} + \frac{1}{2} \frac{1}{r} \frac{\partial V_{\theta j}^2}{\partial \theta} + \frac{V_{\phi j}^2}{R} \sin\theta \right] \tag{17}$$

and

$$\left[\nabla \cdot \Pi_j \right]_\theta = \eta_{0j} \left(\frac{1}{2} A_{oj} \right) \left\{ \frac{1}{r} \frac{\partial \ln\left(\eta_{0j} A_{oj} \right)}{\partial \theta} - 3 \frac{\sin\theta}{R} \right\} \tag{18}$$

where M and F represent external momentum input from the neutral beam injection and interspecies collisional friction, respectively. We note that the "parallel" component of the viscosity enters the rotation calculation at this point and ultimately affects the calculation of the poloidal asymmetry factors

$\tilde{\theta}_j$ which enter into the calculation of the frequencies v_{dj} for the radial transport of toroidal angular momentum.

Making expansions of the type indicated by Eq.(11) for the density and velocities for each species in Eq. (16) and taking the flux surface average with weighting functions 1, $sin\theta$ and $cos\theta$ results in a coupled set of moments equations (three times the number of ion species) that must be solved for the $V_{\theta j}^0$ and $\tilde{n}_j^{s,c}$ for all the plasma ion species. If the first term on the right in Eq. (17) is neglected, these equations can be solved locally on each radial flux surface. The justification for this neglect is the plausible assumption $V_{rj} << V_{\theta j} < V_{\phi j}$, which would also justify neglect of the second term on the right in Eq. (17). The resulting equations are

$$
\begin{aligned}
&\overline{V}_{\theta j}\left[-q\overline{V}_{\phi j}\,\varepsilon\left(\tilde{n}_j^s+\overline{\Phi}^s\right)-q^2 f_j f_p\left(1+\overline{\Phi}^c+\frac{2}{3}\tilde{n}_j^c\right)+f_p\sum_{k\neq j}\nu_{jk}^*(1+\Delta_{fric,j})\right]\\
&-\sum_{k\neq j}\overline{V}_{\theta k}\left[f_p\nu_{jk}^*\sqrt{\frac{m_j}{m_k}}\right](1+\Delta_{fric,k})=\\
&-\overline{V}_{rj}-q\varepsilon\frac{1}{4}\tilde{n}_j^s-q\varepsilon\overline{\Phi}_j\left[\frac{1}{4}\left(\overline{\Phi}^s+\Delta_{\Phi j}\right)\right]-q^2 f_j f_p\left(\overline{V}_{\phi j}+\overline{P}_j'\right)\overline{\Phi}^c\\
&-q\varepsilon\overline{V}_{\phi j}\left[\left(\overline{V}_{\phi j}+\overline{P}_j'\right)\overline{\Phi}^s+\frac{1}{2}\overline{V}_{\phi j}\tilde{n}_j^s\right]
\end{aligned}
\tag{19}
$$

where $\Delta_{fric,j}\equiv-\frac{1}{2}\varepsilon^2\left(1+n_j^c+\left(n_j^c\right)^2+\left(n_j^s\right)^2\right),\Delta_{\Phi j}\equiv\tilde{n}_j^c\overline{\Phi}^s-\tilde{n}_j^s\overline{\Phi}^c$, and

$$
\begin{aligned}
&\tilde{n}_j^s\left[\frac{1}{3}\frac{q^2}{\varepsilon}f_j f_p\overline{V}_{\theta j}+\frac{1}{2}\varepsilon\overline{V}_{rj}-\frac{1}{2}\varepsilon f_p\sum_{k\neq j}\nu_{jk}^*\overline{V}_{\theta k}\sqrt{\frac{m_j}{m_k}}\right]\\
&+\tilde{n}_j^c\left[\frac{1}{2}qf_p^2\overline{V}_{\theta j}^2-\frac{1}{4}q\right]=-\frac{1}{2}\varepsilon f_p\sum_{k\neq j}\nu_{jk}^*\overline{V}_{\theta j}\tilde{n}_k^s-\frac{1}{2}q\overline{V}_{\phi j}^2(1+\Delta_{inert1,j})\\
&+\frac{1}{4}q\overline{\Phi}_j\overline{\Phi}^c-\frac{q^2}{\varepsilon}f_j f_p\frac{1}{2}\left(\overline{V}_{\theta j}-\overline{V}_{\phi j}-\overline{P}'_j\right)\overline{\Phi}^s-\frac{1}{2}qf_p^2\overline{V}_{\theta j}^2
\end{aligned}
\tag{20}
$$

where $\Delta_{inert1,j}=\frac{1}{2}\varepsilon^2\left(\frac{1}{2}\left(\overline{V}_{\phi j}^c\right)^2+\tilde{n}_j^c\overline{V}_{\phi j}^c+3\tilde{n}_j^s\overline{V}_{\phi j}^s+\frac{3}{2}\left(\overline{V}_{\phi j}^s\right)^2\right)$, and

$$
\begin{aligned}
&\tilde{n}_j^c\left[\frac{1}{3}\frac{q^2}{\varepsilon}f_j f_p\overline{V}_{\theta j}+\frac{1}{2}\varepsilon\overline{V}_{rj}-\frac{1}{2}\varepsilon f_p\sum_{k\neq j}\nu_{jk}^*\overline{V}_{\theta k}\sqrt{\frac{m_j}{m_k}}\right]\\
&+\tilde{n}_j^s\left[-\frac{1}{2}qf_p\overline{V}_{\theta j}^2+\frac{1}{4}q\right]=-\frac{1}{2}\varepsilon f_p\sum_{k\neq j}\tilde{n}_k^c\left[\nu_{jk}^*\overline{V}_{\theta j}\right]\\
&-\frac{1}{4}q\overline{\Phi}_j\overline{\Phi}^s-\frac{q^2}{\varepsilon}f_j f_p\left[\frac{1}{2}\left\{\left(1+\overline{\Phi}^c\right)\overline{V}_{\theta j}-\left(\overline{V}_{\phi j}+\overline{P}_j'\right)\overline{\Phi}^c\right\}\right]\\
&-q\overline{V}_{\phi j}^2\Delta_{inert2,j}
\end{aligned}
\tag{21}
$$

where $\Delta_{inert2,j} = \frac{1}{4}\varepsilon\left\{\tilde{V}^{s}_{\phi j}\tilde{V}^{c}_{\phi j} + \tilde{n}^{c}_{j}\tilde{V}^{s}_{\phi j} + \tilde{n}^{s}_{j}\tilde{V}^{c}_{\phi j}\right\}$. The $\tilde{V}^{s,c}_{\phi j}$ are derived from the radial component of the momentum balance equation and defined in Eq. (13). We note that $V^{c}_{\theta j}/V^{0}_{\theta j} = -\varepsilon\left(1+\tilde{n}^{c}_{j}\right)$ and $V^{s}_{\theta j}/V^{0}_{\theta j} = -\varepsilon\left(\tilde{n}^{s}_{j}\right)$ have been derived from the particle continuity equations and used in the above development. We have introduced the additional notation

$$\tilde{V}_{rj} \equiv \frac{\overline{V}_{rj}}{\left(\frac{m_j \upsilon_{thj}}{e_j B^0_\theta}\right)\left|f_p\right|\left(\frac{\upsilon_{thj}}{qR}\right)}, \qquad \nu^{*}_{jk} \equiv \frac{\overline{\nu}_{jk}}{\frac{\upsilon_{thj}}{qR}}, \qquad \tilde{\Phi}_j \equiv \frac{e_j\overline{\Phi}}{T_j}, \tag{22}$$

The Δ_{xx} are higher order terms that were not consistently retained in earlier versions (e.g. Ref. 24) of these equations.

E. Radial electric field and toroidal rotation velocities

For each ion species, the momentum balance equation minus $m_j\mathbf{V}_j$ times the particle balance equation is

$$n_j m_j\left(\mathbf{V}_j\cdot\nabla\right)\mathbf{V}_j + \nabla p_j + \nabla\cdot\Pi_j = -n_j e_j\nabla\Phi + n_j e_j\mathbf{V}_j\times\mathbf{B} + \mathbf{F}_j + \mathbf{M}_j \tag{23}$$

where $\mathbf{F}_j = -n_j m_j \nu_{jk}\left(\mathbf{V}_j - \mathbf{V}_k\right)$ is the interspecies collisional friction and $\mathbf{M}_j$ is the net external momentum input (e.g. neutral beam input less any charge-exchange and asymmetric ionization source losses). The lowest-order radial component of the flux surface average of Eq. (23) for each species 'j' is

$$\left(\overline{E}_r \Big/ B^0_\theta\right) = V^0_{\phi j} - \left(B^0_\phi \Big/ B^0_\theta\right)V^0_{\theta j} + \overline{P}'_j \tag{24}$$

where the overbar or zero superscript indicates the average value over the flux surface.

The flux surface average of the toroidal component of Eq. (23) for each species 'j' can be written

$$n^0_j m_j \overline{\nu}_{jk}\left(\left(1+\beta_j\right)V^0_{\phi j} - V^0_{\phi k}\right) = n^0_j e_j E^A_\phi + e_j B^0_\theta \Gamma_j + \overline{M}_{\phi j} \equiv n^0_j m_j \overline{\nu}_{jk} y_j, \tag{25}$$

where radial transport of toroidal momentum is represented by the parameter

$$\beta_j \equiv \frac{\overline{\nu}^{*}_{dj}}{\overline{\nu}_{jk}} \tag{26}$$

The ion-electron friction term has been neglected. A sum over other species 'k' is implied and the collisional momentum conservation requirement $n^0_j m_j \overline{\nu}_{jk} = n^0_k m_k \overline{\nu}_{kj}$ has been used in deriving Eq. (25).

We note that most neoclassical derivations (e.g. Refs. 14 and 27) obtain the result that the radial electric field is proportional to the radial ion temperature gradient (which is proportional to V_θ in those derivations). The above equations can be rearranged to compare with these earlier derivations. Using the radial momentum balance Eqs. (24) in the toroidal momentum balance Eqs.(25) to eliminate the $V^0_{\phi j}$ and summing over species yields another expression for the radial electrostatic field

$$\frac{\overline{E}_r}{B^0_\theta} = \begin{bmatrix} \{\tilde{M}_{\phi I} + \overline{M}_{\phi i}\} + \beta_i\{\overline{P}'_i - \left(B^0_\phi \Big/ B^0_\theta\right)\left(V^0_{\theta i}\right)\} + \\ \beta_I\{\overline{P}'_I - \left(B^0_\phi \Big/ B^0_\theta\right)\left(V^0_{\theta I}\right)\} \end{bmatrix} \div \left[\beta_i + \beta_I\right] \tag{27}$$

that displays the dependence on momentum input, pressure and poloidal rotation velocity. Since earlier derivations usually do not take into account the presence of external angular momentum input they naturally do not obtain the terms in the first { } brackets.

III. Comparison with DIII-D rotation measurements

The main purposes of this paper are to compare theoretical and experimental toroidal rotation velocity radial profiles and to draw some conclusions therefrom about how much of the radial transport of toroidal angular momentum in DIII-D tokamak plasmas is accounted for by neoclassical viscosity (as represented in the previous section) and how much must be attributed to other processes. A diverse set of discharges including L- and H-modes, with and without internal transport barriers and with and without neon injection, were analyzed for this purpose, as indicated in Table 1. The measured density and temperature profiles for these shots are given in Figs. 1 and 2. A secondary purpose was to extend the investigation of the effect of neon impurity injection on momentum transport, for which purpose three "sister shot" pairs with and without neon injection were included.

A. Description of discharges

L-mode"sister shots" 98777 and 98775 @ 1.6s[40]

These were L-mode shots that were operated identically in every respect except for the injection of 2.8% neon impurity concentration in shot 98775. Long wavelength turbulence as well as heat and momentum transport were measured to be reduced with neon-injection. The intrinsic carbon concentrations were 1.1% in #98777 and 0.5% in the neon-injected #98775. (The cited carbon and neon concentrations correspond to the measured values at $\rho = ½$ in this and other shots.)

L-mode ITB "sister shots" 102942 and 102940 @ 1.4s[41]

These were co-injected shots with an internal transport barrier (ITB) and a typical L-mode edge. The measured temperature and toroidal velocity profiles were quite peaked throughout the discharge. The density profiles were flat early in the discharge, but sharp density and electron temperature gradients developed later in the discharge following an increase in beam power, indicating the formation of an internal transport barrier (ITB). The shots were operated identically except for neon injection in shot 102940, which produced broader profiles and higher temperatures (i.e. better energy confinement), larger toroidal rotation velocities, and reduced turbulence levels in the core as compared to the sister shot 102942 without neon injection.

H-mode shot 99411 @ 1.8s[42]

This was a high-performance ($H_{89P} = 2.8$, $\beta_N H_{89P} = 10$) ELMing H-mode shot with a typical H-mode edge pedestal and a relatively large (5%) carbon intrinsic impurity concentration.

H-mode QDB "sister shots" 106919 @ 3.5s & 106972 @ 2.9s[43]

These were counter-injected, quiescent double barrier (QDB) shots with both an internal transport barrier and an edge transport barrier typical of H-mode discharges. The edge was quiescent [i.e. free of edge localized modes (ELMs)], but a saturated coherent MHD edge harmonic oscillation (EHO) was present at the separatrix. The turbulence was reduced but not entirely suppressed in the internal transport barrier. These discharges had relatively low plasma densities and large and accumulating concentrations of Ni and Cu (Z_{eff} at $\rho = ½$ was 4.1 @ 2010 ms and 5.4 @ 3510 ms, more than half of which was due to Ni and Cu). The carbon concentration was 3.7% in 106919 and 3.1% in 10697. The shots were operated identically except for neon injection in shot 106972.

B. "2-Species" calculation model

The calculation model consisted of Eqs. (19)-(21) for the poloidal rotation velocities and density asymmetries for the main ion (deuterium) and an effective impurity ion species, the two Eqs. (25) for the

toroidal rotation velocities for the main and effective impurity ion species, and the radial component Eq. (24) of the momentum balance for the effective impurity species. We solved the two Eqs. (25) for the deuterium ion rotation velocity

$$V_{\phi i}^{0} = \frac{(1+\beta_I)\, y_i + y_I}{(1+\beta_i)(1+\beta_I) - 1} \tag{28}$$

and then solved the deuterium ion Eq. (25) for the effective impurity rotation velocity

$$V_{\phi I} = (1+\beta_i) V_{\phi i} - y_i \tag{29}$$

The radial electric field was then calculated from the radial momentum balance Eq. (24) for the effective impurity species, for consistency with the way the experimental radial electric field was calculated.

C. Evaluation of input parameters

We took the electron density distribution, the ion and electron temperature distributions, the toroidal electric field, and the radial gradient scale lengths L_n^{-1}, L_T^{-1} and L_v^{-1} from experiment. The radial distribution of neutral beam angular momentum deposition was calculated with the code NBEAMS[44]. The value of the electrostatic potential Φ used in Eq. (19) to calculate the poloidal rotation velocity was taken from TRANSP calculations[45] based on an integration inward of the experimental radial electric field. The calculation was only made out to ρ = 0.9 or 0.95 because atomic physics effects (not taken into account in the calculation) become an important momentum transfer mechanism closer to the separatrix.

A brief discussion of the use of the experimental radial gradient scale lengths L_n^{-1}, L_T^{-1} and L_v^{-1} is in order at this point so that their effect on the calculation is clear. Our intent in this paper is to test the validity of Eq. (9) and its approximate representation Eq. (12), the expression for the gyroviscous torque which determines the rate of radial transport of toroidal angular momentum. The radial derivatives enter Eq. (12) via the factor G_j. We are not able at this time to accurately calculate the radial distributions of *n, T* and V_φ needed to accurately evaluate G_j, yet the accurate evaluation the G_j is a necessary (but not sufficient) condition for Eq. (12) to predict the correct momentum transport rate. So we use the experimental gradient scale lengths to insure that an accurate evaluation of G_j is used to test Eq. (12). To put it another way, to calculate the correct momentum transport rate it is not only necessary to use the correct G_j, but also to use it in the correct equation, to use the correct viscosity coefficient $\eta = \eta_4 = nmT/ZeB$ and poloidal asymmetry factor given by Eq. (11). E.g., if Eq. (10) for the perpendicular viscosity with $\eta = \eta_2 = \left(nmT/ZeB\right)/\Omega\tau$ was used instead of Eq. (9) to represent the radial transport of toroidal angular momentum, and if the same experimental radial gradient scale lengths were used to evaluate the expression equivalent to Eq. (12) derived from Eq. (10), the resulting magnitude of the toroidal rotation velocity would be several orders of magnitude larger because $\Omega\tau \approx 10^3 - 10^4$.

In a similar vein, we have elected to use the value of the electrostatic potential Φ calculated in TRANSP by integrating the experimental radial electric field, rather than integrating the calculated radial electric field, because there is some ambiguity about the boundary conditions that should be used.

D. Modeling of multiple impurity species

Since the present model is limited (by implementation, not inherently) to two ion species—"main ion" and "impurity"—it was necessary to model the six charge states of carbon as a single impurity species with effective charge and mass determined by density weighting. This should be a good approximation over most of the plasma where carbon is fully ionized, but not in the edge. When neon was present it was similarly treated, and then the effective neon and carbon species were combined into a single effective impurity species. In the counter-injected shots with significant Cu and Ni impurities a similar treatment was used to obtain a single high-Z (Ni+Cu) impurity that was then combined with carbon and neon to obtain a single effective impurity species. (This single impurity species model was

found to cause the calculation to become inconsistent for the shots with multiple high-Z impurity charge states, as will be discussed.) Clearly, the association of the calculated "impurity" rotation velocity with the measured carbon VI rotation velocity in the presence of neon and high-Z impurities is valid only to the extent that the various impurity ion species are entrained by interspecies collisions to have a common rotation velocity, which is thus an implicit assumption of this work. We plan to introduce a multiple impurity species model in future work. Note that the less collisional main (deuterium) ions are not assumed to have the same rotation velocities as the more collisional impurity ions.

E. Numerical solution

Taking Eqs. (19)-(21) (for each species) and Eqs. (28)-(29) as our model for a two-species plasma of ions and impurities, we have an 8-dimensional system of coupled nonlinear equations. We solved this set of nonlinear equations for the rotation velocities and poloidal density coefficients $\left(V_{\phi i}, V_{\phi I}, V_{\theta i}, V_{\theta I}, n_i^c, n_I^c, n_i^s, n_I^s\right)$ numerically. A scalar residual merit function over the unknown parameters was defined as the magnitude of the vector of the normalized residuals, and was evaluated at each radial location. The residual for each equation was the value of the equation, when all terms were collected to one side, using the parameter values as the trial solution, and was normalized by the root-mean-square of the individual terms. The merit function was minimized using a simplex search algorithm[46,47]. Solutions were generally accepted as converged only if the scalar residual was on the order of 10^-11 or less, though some few points were accepted with somewhat larger values if they were seen to be a continuation along the radius of accepted solutions at other radii.

F. Comparison of calculated and measured toroidal rotation frequencies

The measured and calculated toroidal rotation frequencies $\Omega_\phi \equiv V_\phi / R$ are compared in Figs. 3a-9a. The corresponding poloidal rotation velocities are shown in Figs. 3b-9b, the density asymmetry coefficients of Eq. (11) are shown in Figs. 3c-9c, and the radial electric fields calculated from Eq. (24) using the rotation velocities calculated for the effective impurity species are compared with the E_r^{exp} calculated from the same equation using the measured rotation velocities for carbon VI in Figs. 3d-9d. It was not possible to find "accepted" solutions (as discussed above) to the coupled set of nonlinear equations described above at each radial location for all shots. This does not mean necessarily that such solution do not exist, only that they were not found.

For the L-mode shots 98775 and 98777 shown in Figs. 3 and 4, the toroidal rotation frequency is over-predicted by a factor of 1.5-3 in the center region, reducing with radius to rather good agreement in the outer region. The normalized density asymmetry coefficients satisfied $-1 \le n^{c,s} \le 1$, indicating that the effective impurity species model and low-order Fourier expansion model was adequate, except for $\rho > 0.8$ in shot 98775 with neon. This difficulty probably arises from the inadequacy of a single effective impurity species representation of 10 neon charge states in the edge of shot 98775, not from the inadequacy of the low order Fourier expansion per se. The predicted radial electric field, calculated with Eq. (24) using the measured carbon VI pressure gradient and the calculated toroidal and poloidal rotation velocities of the effective impurity species, compares well with the "experimental" radial electric field, also calculated from Eq. (24) using the measured carbon VI pressure gradient but the measured toroidal and poloidal rotation velocities of carbon VI, for shot 98777 without neon, but the agreement is not so good for shot 98775 with neon. This disagreement is related to the larger poloidal rotation velocity calculated for the effective impurity species in shot 98775 with neon. The observed larger toroidal rotation in shot 98775 with neon than in shot 98777 is not apparent in the calculated results.

For the L-mode ITB shots 102940 and 102942 shown in Figs. 5 and 6, the predicted toroidal rotation frequencies for the effective impurity species agree quite well with the measured values for carbon VI (< 50% over-prediction), for those radii at which it was possible to obtain a solution of the nonlinear set of equations. Again, the density asymmetry coefficients satisfied $-1 \le n^{c,s} \le 1$ except for the effective impurity species coefficients in the outer regions of shot 102940 with neon. The calculated radial electric field agreed much better with the measured value for the shot 102942 without neon than for the shot 102940 with neon, and this latter can be attributed to the larger poloidal rotation velocity calculated for the effective impurity species in the shot 10940 with neon. Because of the difficulty in

getting solutions in the inner regions it is not possible to comment on the dependence on neon of the predicted toroidal rotation velocities.

For the H-mode shot 99411 shown in Fig. 7, the predicted toroidal rotation frequencies are a factor of < 3 larger than the measured values. The normalized density asymmetry coefficients satisfied -1 $\leq n^{c,s} \leq 1$. The measured and calculated radial electric fields do not agree in the outer region where a large negative peak in the calculated carbon poloidal rotation causes a negative peak in the calculated E^I_{rad}. This peaking in E^I_{rad} and $V_{\theta I}$ is correlated with a peaking in $n_I^{c,s}$.

Agreement between predicted and measured toroidal rotation frequencies is poorest for the counter-injected QDB shots 106919 and 106972. These shots had significant Cu and Ni impurities, and the normalized density asymmetry coefficients for the effective impurity species were $n^{c,s} \geq 1$ over much of the radius, probably reflecting the inadequacy of treating such a large number of impurity charge states as a single effective species. The disparity in the calculated and measured toroidal rotation velocities is reflected in the disparity between calculated and measured radial electric fields.

So, what can be inferred about the ability of neoclassical gyroviscosity to account for the experimentally inferred radial transport rate of angular momentum? Considering only the shots with only carbon impurities (98777, 102942, 99411), for which the single effective impurity species model would be expected to work the best, we observe that neoclassical gyroviscosity leads to an over-prediction of the toroidal rotation by less than a factor of 2-3 at the most, from which we conclude that neoclassical gyroviscosity can account for one-third to one-half of the experimentally inferred radial transport of toroidal angular momentum in these shots. Considering next the shots with carbon and neon impurities (98775, 102940), there is evidence from the density asymmetries that the single effective impurity species model breaks down for $\rho > 0.8$, where multiple neon charge states are present. The toroidal rotation in these shots is generally over-predicted by only about 50% or less for $\rho < 0.8$, where the single effective impurity species model might be expected to work better, from which we conclude that neoclassical gyroviscosity can account for perhaps 2/3 of the experimentally inferred transport rate of angular momentum in these shots. Finally, consider the QDB shots (106919, 106972), in which multiple charge states of Ni and Cu, together with fully stripped carbon and neon are present throughout the plasma. The poloidal density coefficients indicate that the single effective impurity species model is breaking down over most of the plasma, so these shots do not provide a meaningful test of the ability of neoclassical gyrovicosity to account for the experimentally inferred transport rate of angular momentum. In summary, we conclude that about 1/3 to 2/3 of the experimentally inferred radial transport rate of angular momentum can be accounted for by neoclassical gyroviscosity.

Angular momentum outward convection was not modeled, and including this process would reduce the central peaking in the predicted toroidal rotation frequencies, bringing them into better agreement with measured values, and would account for some additional fraction of the experimentally inferred radial transport rate of toroidal angular momentum.

In addition to the shortcomings of the single effective impurity species representation of multiple impurity charge states discussed above, there are other modeling approximations and assumptions that could affect the above comparison. First, the magnetic flux surface approximation $B = B^0/(1+\varepsilon\cos\theta)$ neglects Shafranov shift, elongation and geometry-driven up-down asymmetry effects due to a single-null divertor. It is expected that taking into account up-down asymmetry in the magnetic field would increase the up-down asymmetry in the density and rotation velocities, which in turn would increase the asymmetry factor of Eq. (13) and hence the gyroviscous momentum transport frequency ν_d defined in Eq. (12). This would presumably result in an increase in the fraction of the experimentally inferred momentum transport rate that is accounted for by neoclassical gyroviscosity. Second, the Braginskii large rotation ordering $V_\phi/\upsilon_{th} \approx 1$ was used in the gyroviscosity representation. The parameter V_ϕ/υ_{th} varied over the range 0.1-0.4 for deuterium in these shots (with larger values for the impurities), so that the Braginskii ordering $V_\phi/\upsilon_{th} \approx 1$ used in this paper seems more appropriate than the Mikhailovski-Tsypin ordering $V_\phi/\upsilon_{th} \ll 1$, but we can not rule out that the gyroviscous stress tensor should be modified to include heat flux terms[27] that are needed in the ordering $V_\phi << \upsilon_{th}$.

IV. Summary and Conclusions

We have tested the neoclassical viscosity formalism for the radial transport of angular momentum by comparing predicted and measured radial profiles of toroidal rotation velocity in several DIII-D discharges spanning L-mode, L-mode with ITB, H-mode and H-mode with QDB confinement regimes with and without neon injection. The velocity calculations were based on using the neoclassical toroidal gyroviscous torque in equations for the toroidal velocities derived from toroidal momentum balance, and on using the neoclassical parallel viscosity in equations for the poloidal rotation velocities and poloidal asymmetries in density and rotation velocities derived from poloidal momentum balance. Measured background temperatures and densities were used, and radial gradients of temperature, density and toroidal velocity were evaluated using radial gradient scale lengths determined from experiment, but otherwise the calculations were "first-principles".

The calculated toroidal rotation over-predicted the measured values in all cases, more in the center of the plasma (by factors of 1.5 to 3) than in the outer regions. We conclude from this that neoclassical viscosity can account for a significant part, but not all, of the radial transport of angular momentum observed in these shots. Several approximations in the calculation model—neglect of convection, one effective impurity species representation, $B_\theta = B_\theta^0 / \left(1 + \varepsilon \cos\theta\right)$ representation of flux surface geometry—prevent us from unambiguously attributing this over-prediction entirely to the presence of other angular momentum transport (e.g. turbulence) or reverse torque input mechanisms.

We intend to improve the calculation model to remove these limitations on its implementation. In addition, we plan to implement a radial differential equation solution for the toroidal velocity profile, thereby removing the necessity of representing radial gradients by gradient scale lengths and taking convection and inertial effects into account automatically.

References

1. S. Suckewer, H. P. Eubank, R. J. Goldston, *et al*., Phys. Rev. Lett., 43, 207 (1979).
2. R. C. Isler, L. E. Murray, E. C. Crume, *et al*., Nucl. Fusion, 23, 1017 (1983).
3. R. J. Groebner, W. Pfeiffer, F. P. Blau, *et al*., Nucl. Fusion, 26, 543 (1986).
4. S. D. Scott, V. Arunasalam, C. W. Barnes, *et al.*, Phys. Fluids B, 2, 1300 (1990).
5. H. P. L. deEsch, D. Stork and H. Weisen, Proc. Conf. Control. Fusion & Plasma Heating (Amsterdam), vol 14B, Part I (Geneva: Euro. Phys. Soc.) p90 (1990).
6. F. Wagner, F. Ryter, A. R. Field, *et al*., Proc. 13th Int. Conf. Plasma Phys. Control. Fusion Res., Washington (Vienna: Int. Atomic Energy Agency) p277 (1991).
7. K-D. Zastrow, *et al*., Proc. 22nd Euro. Conf. Control. Fusion Plasma Phys. (Bournemouth) vol 19C, part II (Geneva: Euro. Phys. Soc.) p453 (1995).
8. J. S. deGrassie, *et al*., Proc. 26th Euro. Conf. Control. Fusion Plasma Phys. (Maastricht) vol 23J (Geneva:Euro. Phys. Soc.)p1189 (1999).
9. K-D. Zastrow, W. G. F. Core, L-G. Erickson, *et al*., Nucl. Fusion, 38, 257 (1998).
10. J. S. deGrassie, D. R. Baker, K. H. Burrell, *et al*., Nucl. Fusion, 43, 142 (2003).
11. A. N. Kaufmann, Phys. Fluids, 3, 610 (1960).
12. S. I. Braginskii, Rev. Plasma Phys., 1, 205 (1965).
13. M. N. Rosenbluth, P. H. Rutherford, J. B. Taylor, *et al*., Proc. Conf. Plasma Phys. Control. Fusion (Vienna: Int. Atomic Energy Agency) vol. 1, p495 (1971).
14. R. D. Hazeltine, Phys. Fluids, 17, 961 (1974).
15. K. T. Tsang and E. A. Frieman, Phys. Fluids, 19, 747 (1976).
16. A. B. Mikhailovskii and V. S. Tsypin, Sov. J. Plasma Phys., 10, 51 (1984).
17. W. M. Stacey and D. J. Sigmar, Phys. Fluids, 28, 2800 (1985).
18. F. L. Hinton and S. K. Wong, Phys. Fluids, 28, 3082 (1985).
19. J. W. Connor, S. C. Cowley, R. J. Hastie and L. R. Pan, Plasma Phys. Control. Fusion, 29, 919 (1987).
20. W. M. Stacey, Phys. Fluids B, 4, 3302 (1992).

21. R. D. Hazeltine and J. D. Meiss, "Plasma Confinement", Addison-Wesley, Reading MA (1994), pp 208, 220 and 226.
22. A. L. Rogister, Phys. Plasmas, 1, 619 (1994).
23. H. A. Claassen, H. Gerhauser and A. Rogister, Phys. Plasmas, 7, 3699 (2000).
24. W. M. Stacey, Phys. Plasmas, 8 158 (2001); 9, 3874 (2002); and 11, 3096 (2004).
25. P. J. Catto and A. N. Simakov, Phys. Plasmas, 11, 91 (2004); also, Contrib. Plasma Phys., 44, 83 (2004).
26. S. K. Wong and V. S. Chan, Phys. Plasmas, 11, 3432 (2004).
27. P. J. Catto and A. N. Simakov, Phys. Plasmas, 12, 012501 (2005).
28. D. Nishijima, A. Kallenbach, S. Gunter, et al., Plasma Phys. Control. Fusion, 47, 89 (2005).
29. A.G. Peeters and C. Angioni, Phys. Plasmas 12, 072515 (2005).
30. W. M. Stacey and D. R. Jackson, Phys. Fluids B, 5, 1828 (1993).
31. W. M. Stacey and M. Murakami, Phys. Plasmas, 8, 4450 (2001).
32. W. M. Stacey and J. Mandrekas, Phys. Plasmas, 9, 1622 (2002).
33. W. M. Stacey, A. W. Bailey, D. J. Sigmar and K. C. Shaing, Nucl. Fusion, 25, 463 (1985); W. M. Stacey and D. J. Sigmar, Phys. Fluids, 27, 2076 (1984) and 22, 2000 (1979); and Nucl. Fusion, 19, 1665, (1979).
34. K. H. Burrell, T. Ohkawa and S. K. Wong, Phys. Rev. Lett., 47, 511 (1981).
35. A. Bondeson and D. J. Ward, Phys. Rev. Lett., 72, 2709 (1994).
36. M. S. Chu, J. M. Greene, T. H. Jensen, R. W. Johnson, *et al.*, Phys. Plasmas, 2, 2236 (1995).
37. A. M. Garofalo, M. S. Chu, E. D. Fredrickson, *et al*., Nucl. Fusion, 41, 1171 (2001).
38. E. Hameiri, Phys. Plasmas, 5, 3270 (1998).
39. K. H. Burrell, Phys. Plasmas, 4, 1499 (1997).
40. G. R. McKee, M. Murakami, J. Boedo, G. L. Jackson *et al*., Phys. Plasmas, 7, 1870 (2000); Nucl. Fusion, 41, 317 (2001).
41. E. J. Doyle, C. M. Greenfield, M. E. Austin, *et al.*, Nucl. Fusion, 42, 333 (2002).
42. M. Murakami, H. St. John, T. A. Caspar, *et al*., Nucl. Fusion, 40, 1257 (2000).
43. W. P. West, M. R. Wade, C. M. Greenfield, *et al*., Phys. Plasmas, 9, 1970 (2002).
44. J. Mandrekas, "Physics models and user's guide for the neutral beam module of the SUPERCODE", Georgia Tech Fusion report GTFR-102 (1992), available from National Technical Information Service, NTIS-PB93-121887INZ.
45. R. J. Goldston, "Topics in confinement analysis of tokamaks with auxiliary heating," in *Basic Physical Processes of Toroidal Fusion Plasmas* (Commission of the European Comm. and Monotypia Frachi Citta di Castello, Italy, 1985), Vol 1, EUR 10418 EN.
46. W. H. Press, "Numerical Recipes", Cambridge Univ. Press, Cambridge (1992).
47. T. Rowan, "Functional Stability Analysis of Numerical Algorithms", PhD Thesis, Dept. Computer Sciences, University of Texas at Austin (1990). ftp://www.netlib.org/opt/

Table 1 Parameters of DIII-D shots selected for rotation analysis

Shot (time)	Conf. Mode	P_{nbi} (MW)	$\bar{n}$ (10^{19}/m^3)	n_{carb}/n_e	$\left(n_{neon}/n_e\right)$	$\left(n_{ni,cu}/n_e\right)$	T_{i0}, T_{e0} (keV)	τ_E^{exp} (ms)
98777 1.6s	L	4.5 CO	3.4	0.011	-----	-----	3.5,2.5	66
98775 1.6s	L	4.5 CO	4.1	0.005	0.028	-----	6.3,3.3	90
99411 1.8s	H	9.2 CO	4.8	0.050	-----	-----	8.3,3.9	168
106919 3.5s	H-QDB	9.3 CTR	2.8	0.037	-----	0.005	14.2,4.2	140
106972 2.9s	H-QDB	8.7 CTR	2.9	0.031	0.003	0.003	15.2,4.2	117
102942 1.4s	L-ITB	7.0 CO	2.9	0.016	-----	-----	12.0,4.7	94
102940 1.4s	L-ITB	7.0 CO	3.2	0.006	0.013	-----	9.7,4.1	128

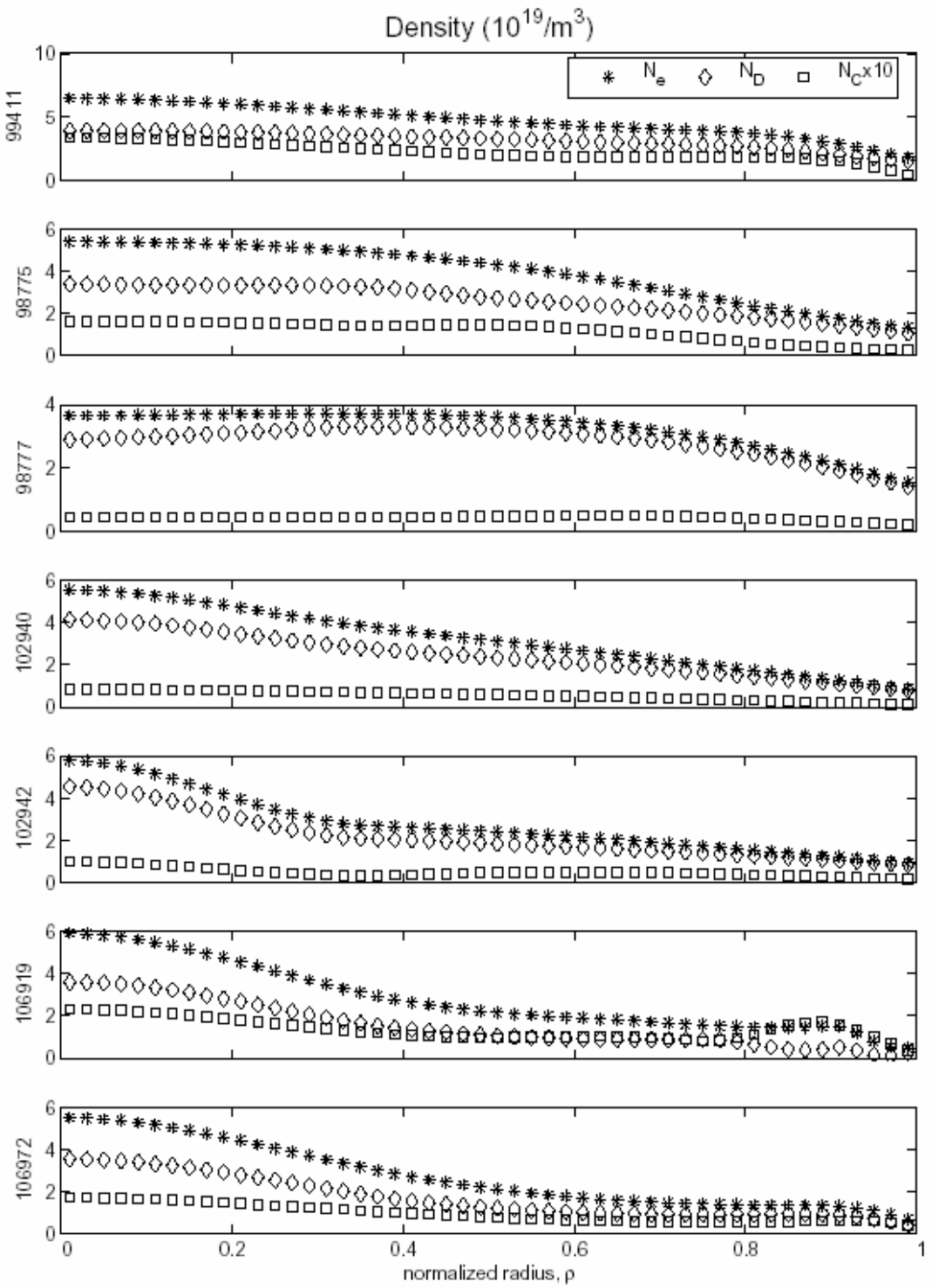

Fig. 1 Experimental electron, deuterium and carbon density distributions.

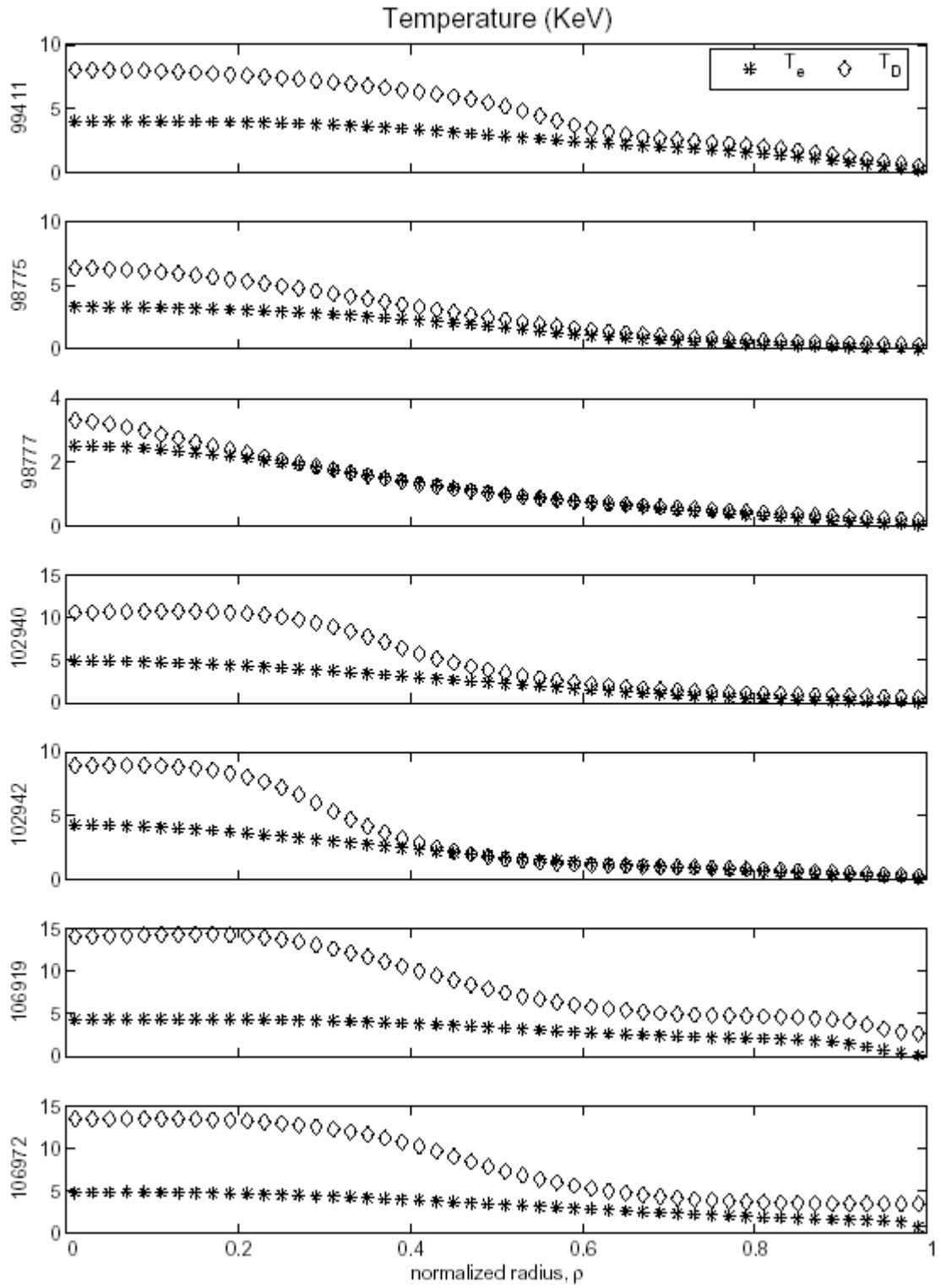

Fig. 2 Experimental deuterium ion and electron temperature distributions.

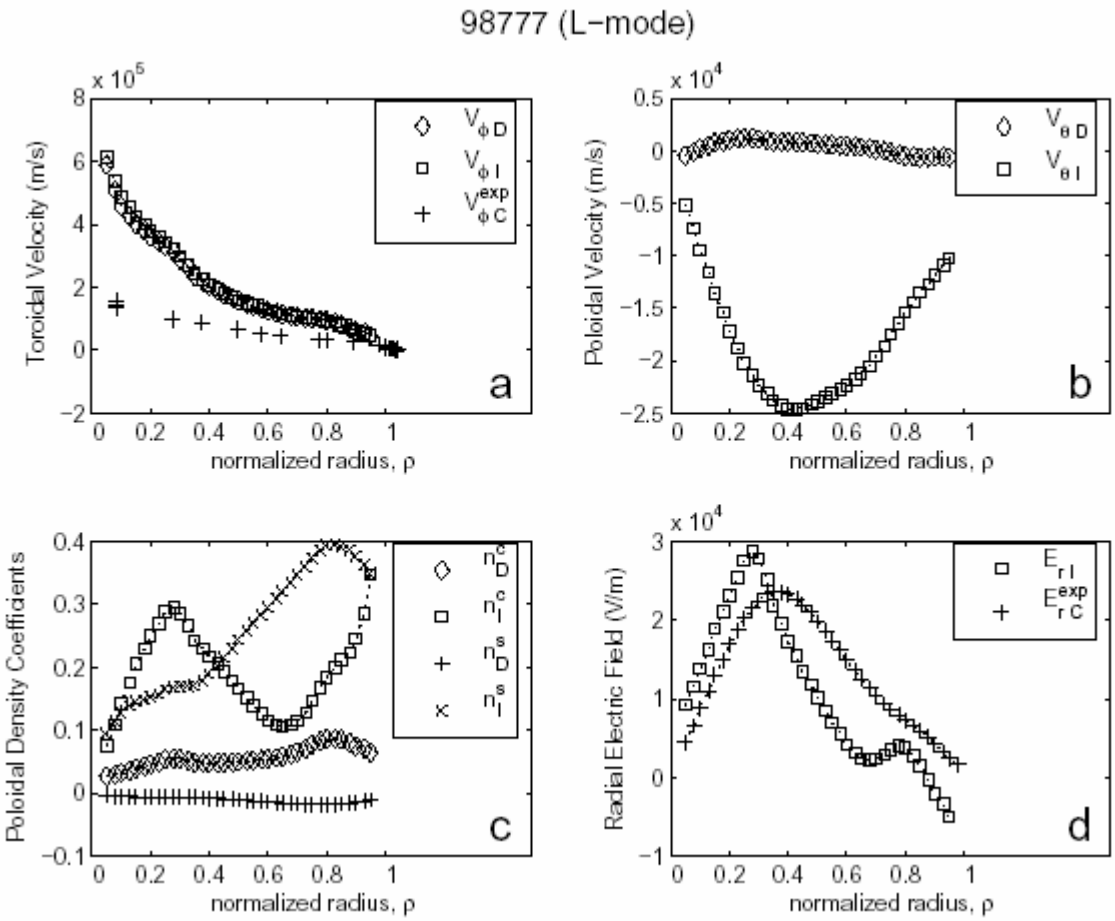

Fig. 3 Rotation calculations and experimental rotation velocities for CO-injected L-mode shot 98777: a) toroidal rotation frequencies $\Omega_\phi \equiv V_\phi / R_0$ for deuterium and carbon; b) poloidal rotation velocities V_θ for deuterium and carbon; c) normalized density asymmetry coefficients $n^{s,c}$ for deuterium and carbon; d) radial electric field from carbon force balance using calculated and experiment $V_{\theta,\phi}$ for carbon.

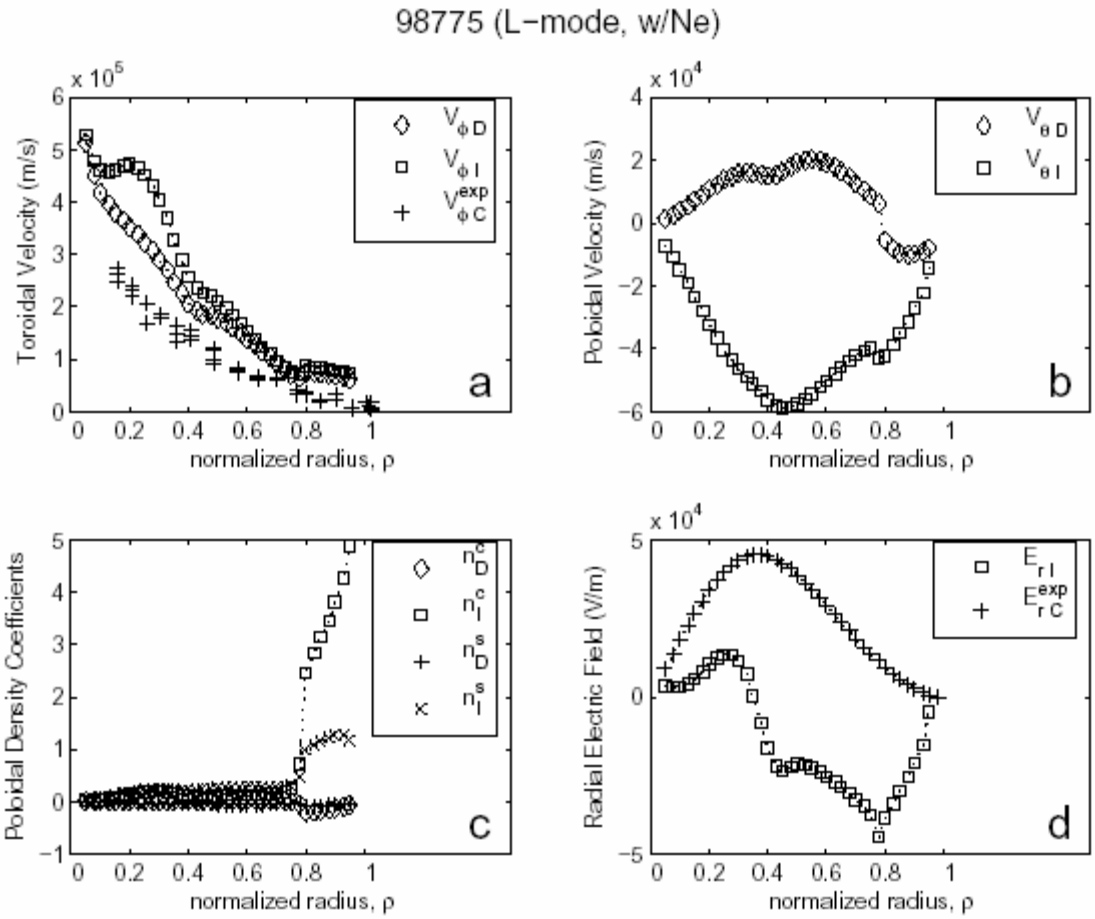

Fig. 4 Rotation calculations and experimental rotation velocities for CO-injected L-mode shot 98775 with neon: a) toroidal rotation frequencies $\Omega_\phi \equiv V_\phi / R_0$ for deuterium and "impurity"; b) poloidal rotation velocities V_θ for deuterium and "impurity"; c) normalized density asymmetry coefficients $n^{s,c}$ for deuterium and "impurity"; d) radial electric field from carbon force balance using calculated $V_{\theta,\phi}$ for "impurity" and experimental $V_{\theta,\phi}$ for carbon.

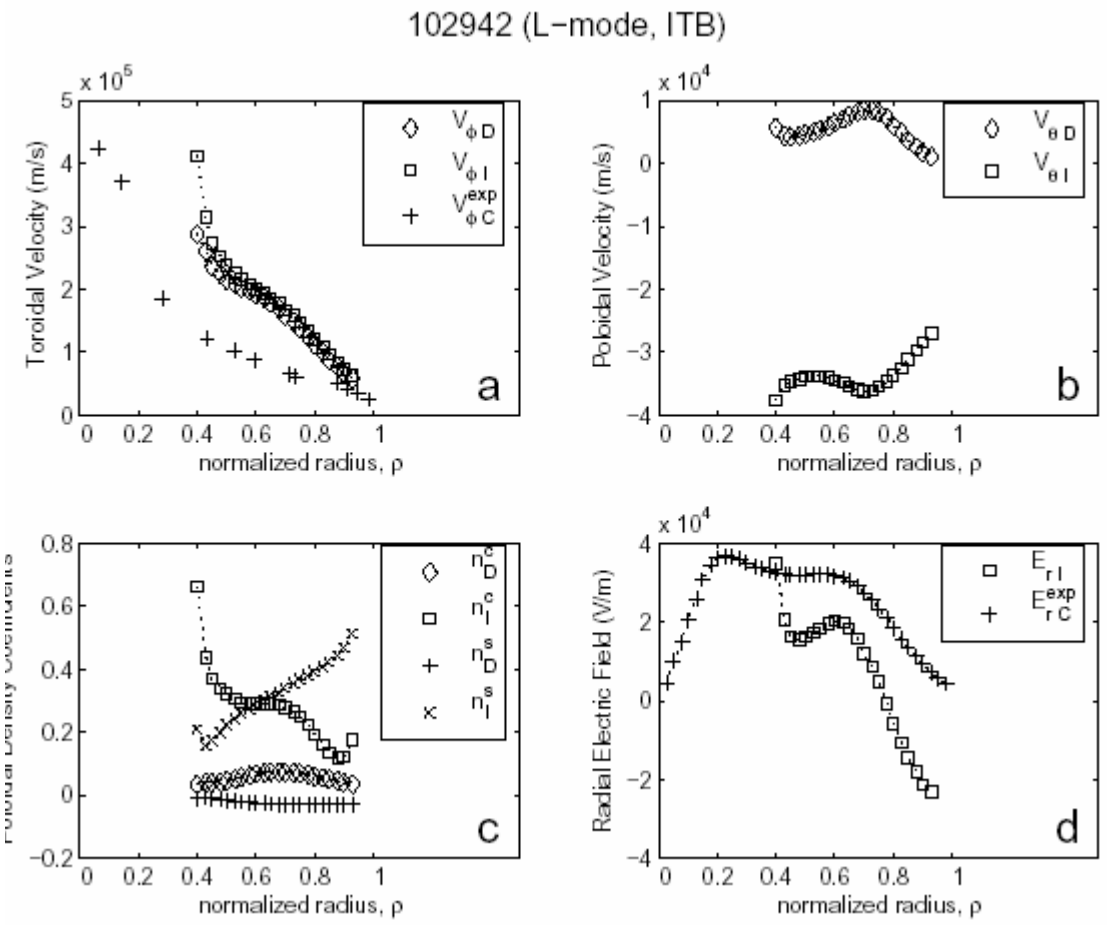

Fig. 5 Rotation calculations and experimental rotation velocities for CO-injected L-mode ITB shot 102942: a) toroidal rotation frequencies $\Omega_\phi \equiv V_\phi / R_0$ for deuterium and "impurity"; b) poloidal rotation velocities V_θ for deuterium and "impurity"; c) normalized density asymmetry coefficients $n^{s,c}$ for deuterium and "impurity"; d) radial electric field from carbon force balance using calculated $V_{\theta,\phi}$ for "impurity" and experimental $V_{\theta,\phi}$ for carbon.

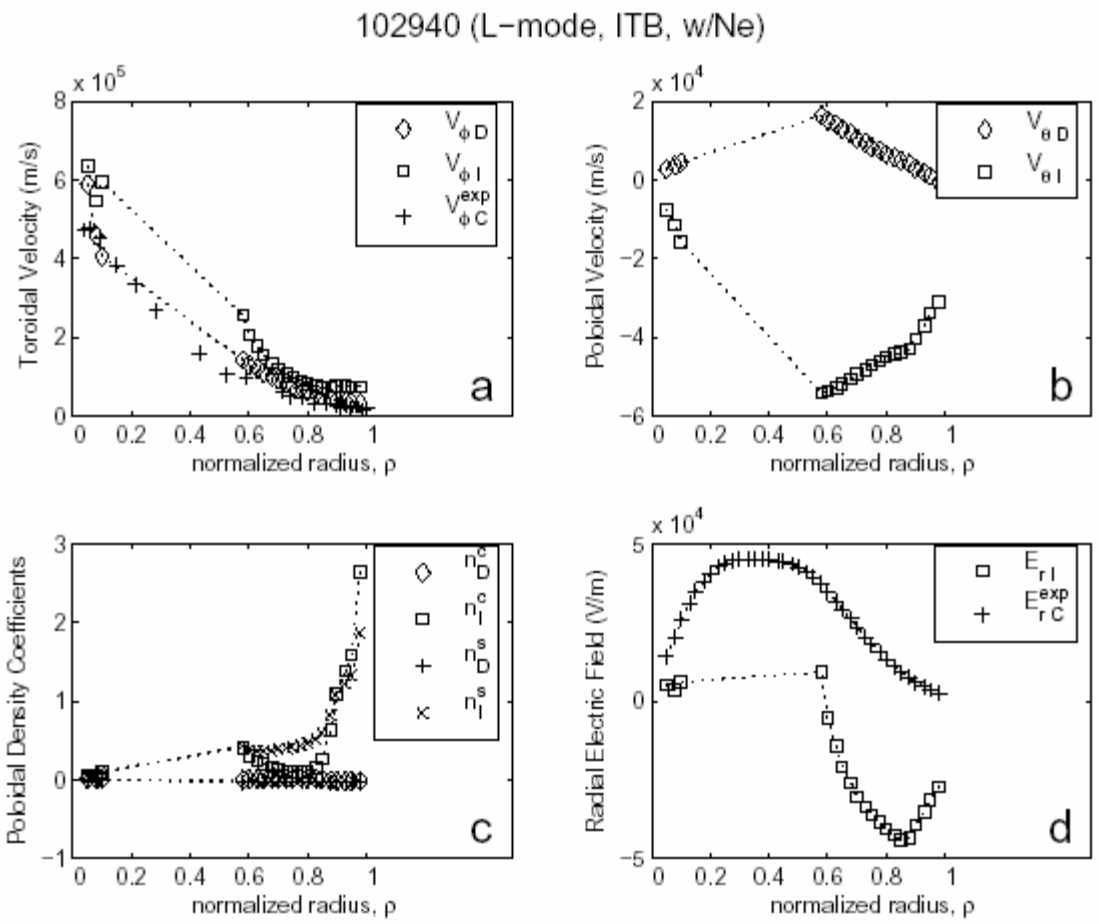

Fig. 6 Rotation calculations and experimental rotation velocities for CO-injected L-mode ITB shot 102940 with neon: a) toroidal rotation frequencies $\Omega_\phi \equiv V_\phi / R_0$ for deuterium and "impurity"; b) poloidal rotation velocities V_θ for deuterium and "impurity"; c) normalized density asymmetry coefficients $n^{s,c}$ for deuterium and "impurity"; d) radial electric field from carbon force balance using calculated $V_{\theta,\phi}$ for "impurity" and experimental $V_{\theta,\phi}$ for carbon.

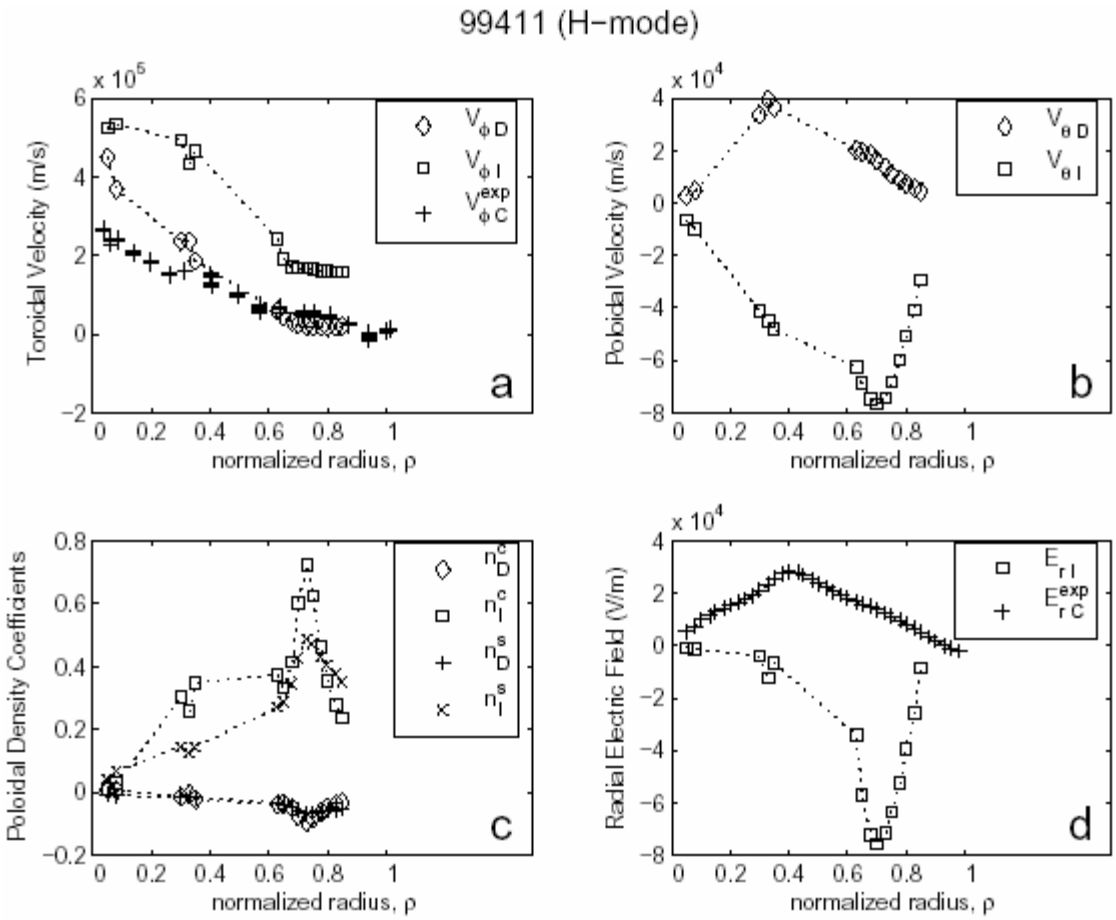

Fig. 7 Rotation calculations and experimental rotation velocities for CO-injected H-mode shot 99411: a) toroidal rotation frequencies $\Omega_\phi \equiv V_\phi / R_0$ for deuterium and carbon; b) poloidal rotation velocities V_θ for deuterium and carbon; c) normalized density asymmetry coefficients $n^{s,c}$ for deuterium and carbon; d) radial electric field from carbon force balance using calculated and experiment $V_{\theta,\phi}$ for carbon.